JOURNAL OF Materials CHEMISTRY
Feature Article

Dynamic neutron and synchrotron X-ray powder diffraction methods in the study of chemical processes

M. C. Morón

Instituto Ciencia Materiales Aragón, CSIC - Universidad de Zaragoza, Pedro Cerbuna 12, E-50009 Zaragoza, Spain. E-mail: nina@posta.unizar.es

Received 5th May 2000, Accepted 28th September 2000
First published as an Advance Article on the web 7th November 2000

The usefulness of *in-situ* neutron and synchrotron X-ray powder diffraction methods is stressed presenting the current possibilities, limitations and potential of these techniques in the study of chemical processes. The opportunity of following the evolution of a chemical phenomenon as a function of an external or internal parameter provides direct information about transformations occurring in the sample during the chemical reaction, thus largely contributing to greater understanding of the complexity of the process. This article intends to reflect the state of the art and its recent impact in materials chemistry with the aim of stimulating further work on this particularly creative and promising field of research. Some parameters optimizing the choice between neutron and synchrotron radiation are also discussed through a number of selected experiments.

1. Introduction

Neutron and X-ray powder diffraction are versatile techniques that have long been considered as convenient, non-destructive, methods for the characterization of materials.[1–3] Applications of these methods can be found in many fields of the physical, chemical and biological sciences. In particular, the possibility of following the evolution of a chemical phenomenon as a function of an external (time, temperature, pressure. *etc.*) or internal parameter (chemical composition, proportion of reactants, *etc.*) can give valuable information about the system under study.[4] This particular dynamic diffraction technique, compared to the static method, yields information about changes occurring in a sample along a chemical process. Rapid changes on diffraction patterns can be observed now in real time due to the development of fast detectors and powerful radiation sources.

Effects that are not relevant for reactions in a fluid medium, like nucleation, particle shape and size, crystal defects or heat conduction, are so significant for reactions in the solid state that they often dominate the whole process. For decades the chemistry of the solid state has received serious criticism due to the classical approach to the involved processes including a lack of knowledge about the reaction mechanisms. The dynamical information of a system obtained from powder diffraction methods can largely contribute to the understanding of the complexity of solid state reactions.[3,5–7] Apart from the possibility of simultaneously identifying all compounds present, the method can provide quantitative and kinetic parameters, clarify the associated reaction mechanisms, detect transient intermediate phases (unnoticed in static experiments) or optimize the conditions for synthesizing a desired material (temperature, reaction times, external pressure, excess of a given reactant, *etc.*) with given properties (grain size, absence of strains, impurities, *etc.*). Moreover, estimation of particle size and strain through the study of the peak shape are essential for analyzing the influence of microstructural effects during chemical reactions and for understanding the mechanisms of transformations at the atomic level.

In contrast to X-rays which are scattered by electrons, neutrons are scattered by atom nuclei. This leads to special applications depending on the nature of the chemical process to be analyzed and the type of information to be obtained. Neutrons present a relatively weak interaction with matter. Most elements of the Periodic Table exhibit a low absorption cross-section concerning neutron scattering. This is of particular importance for the study of chemical reactions since it allows one to study bulk samples and not only their 'surface' as usually happens when using X-ray diffraction methods. Another useful consequence of the low absorption is the notable simplification of the construction of the sample environment such as furnace, reaction cells or cryostats. In addition, the almost random dependence of the neutron scattering amplitude on atomic number clearly renders some advantages in the study of chemical reactions involving mixtures of reactants including light and heavy atoms.

However, the intensity of the radiation provided by synchrotron X-ray sources is orders of magnitude more intense than that from neutron sources. Consequently, synchrotron X-ray diffractometers are potentially able to follow faster dynamical processes and to examine samples with smaller volumes. An adequate study of dynamic chemical processes by diffraction implies that the data acquisition time is short enough compared to the time required to complete the reaction or transformation. The time resolution associated with neutron powder diffraction techniques, typically in the range of minutes and subminutes, is well adapted to many solid state chemical processes which often have times of reaction of around a few hours. However in the cases of faster chemical processes, synchrotron X-ray powder diffraction, with a characteristic time resolution in the range of the second and subsecond, would be in principle a particularly appropriate choice.

In an attempt to introduce the reader to this particular although rare field of research a number of selected experiments are discussed below. Owing to the potential wide range of applications the present article is not intended to review all the areas of research on the subject but to reflect the state of the art and its recent impact in materials chemistry emphasizing the possibilities of the method in an intent to encourage further work on this creative field of research.

2. Transient intermediate phases and reaction mechanisms

Of special relevance is the ability of dynamic diffraction to detect transient intermediates that might otherwise go unno-

DOI: 10.1039/b003604h

ticed in static measurements. Thus, the thermal decomposition of cobalt(II) acetate tetrahydrate, $Co(CH_3CO_2)_2{\cdot}4H_2O$, has been studied using time-resolved powder neutron diffraction.[8] The first step of the process is the loss of the water content which is finished by 150 °C. Crystallization of anhydrous Co(II) acetate starts to occur at 200 °C. Further heating leads to the decomposition of the anhydrous acetate terminated by the formation of CoO between 275–310 °C. Interestingly, after the water ligands have been lost, and before the crystallization of anhydrous acetate, there is a period in which there are no well defined diffraction peaks. The broad undulations of the diffraction intensity that are seen between 160 and 200 °C are typical of a material in a glassy phase.

A question arises: why does the transition between hydrated and anhydrous Co(II) acetate occur *via* an amorphous intermediate? The coordination of the cobalt ion in $Co(CH_3CO_2)_2{\cdot}4H_2O$ is octahedral.[9] The cations are surrounded by four water molecules and by two oxygen ions from unidentate acetate groups. Grimes *et al.*[8] suggest the anhydrous acetate is composed of structural units of $Co_4O(Ac)_6$ where $Ac = CH_3CO_2$. This result is consistent with diffraction, thermogravimetric and chemical analyses. The crystal structure of $Co_4O(Ac)_6$ has not been determined yet. However the structure of related materials such as $Zn_4O(Ac)_6$ is known.[10] The zinc ion is tetrahedrally coordinated by oxygen, one oxygen being the central ion and the other three components of acetate ligands. A possible explanation for the non-crystalline nature of the intermediate phase would be the complete change in the coordination of the cobalt ion, octahedral to tetrahedral, as a consequence of dehydration. The crystal structure determination of $Co_4O(Ac)_6$ would be of interest in order to confirm this hypothesis. A parallel procedure could be followed. The intermediate phase could be produced *in-situ* and isolated by stopping the heating at the correct moment, *i.e.* an *in-situ* synthesis.[11] Once obtained, the phase can be studied by standard *ex-situ* methods.

The mechanism associated with the chemical processes $MoO_3{\cdot}2H_2O \rightarrow MoO_3{\cdot}H_2O \rightarrow MoO_3$ has been studied by performing a real time neutron powder thermodiffractometric experiment.[12] An analysis of the patterns as a function of the temperature shows that the first Bragg peaks of the monohydrated phase appear at $T \cong 60$ °C while $MoO_3{\cdot}2H_2O$ does not vanish before $T \cong 80$ °C. The completely dehydrated compound, MoO_3, starts to form at about 150 °C.

The crystal structure of $MoO_3{\cdot}2H_2O$ is built from slightly distorted layers of corner sharing $MoO_5(H_2O)$ octahedra (Fig. 1). These layers are connected by interlayer water molecules. However, the atomic positions of atoms in $MoO_3{\cdot}H_2O$ were not known. The full refinement of the crystal structure could not be performed since the parameters to be fitted were too many compared with the number of independent reflections collected within a too small angular 2θ range. Nevertheless the distribution of the peak intensities in a calculated pattern from a model deduced from the atomic arrangement of $WO_3{\cdot}H_2O$ was very close to that observed for $MoO_3{\cdot}H_2O$. This model provides a good enough approximation to the real atomic positions of the monohydrate. Thus $MoO_3{\cdot}H_2O$ keeps the water molecule coordinated to the metal ion within the $MoO_5(H_2O)$ octahedra but the interstitial water found in $MoO_3{\cdot}2H_2O$ is no longer present (Fig. 1). Therefore the water molecule lost during the dehydration process $MoO_3{\cdot}2H_2O \rightarrow MoO_3{\cdot}H_2O$ corresponds to that occupying interstitial positions and not to that coordinated to the Mo cation. As a result, the first step of the dehydration in air corresponds to the loss of the interlayer water molecules from the dihydrate leading to $MoO_3{\cdot}H_2O$.

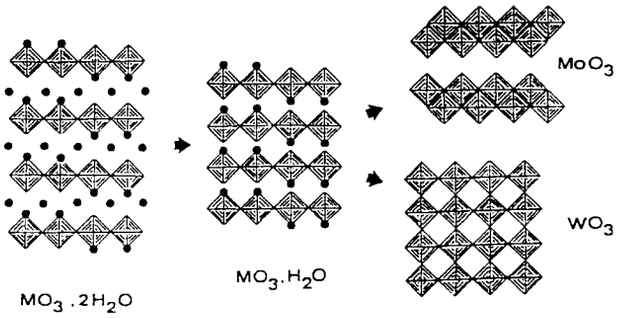

Fig. 1 Scheme of the dehydration process $MoO_3{\cdot}2H_2O \rightarrow MoO_3{\cdot}H_2O \rightarrow MoO_3$ (M represents either Mo or W, see text for details). Reproduced by permission of Academic Press from ref. 12.

The mechanism associated with the second dehydration reaction, $MoO_3{\cdot}H_2O \rightarrow MoO_3$, seems to be more complex than the first one because of the final compact layer structure of MoO_3. The crystal structure of the anhydrous compound is built of bilayers of Mo oxygen octahedra sharing two edges arranged in an orthorhombic cell (Fig. 1). When the water molecules disappear the octahedra collapse following a displacement perpendicular to the layers. This transformation could be explained as well on the basis of processes involving oriented nucleation and growth as explained by Figlarz *et al.*[13] The close study of the crystal structure of the three molybdate products, including the relations between the corresponding cell parameters, define the topotactic character of the mechanism associated with the chemical processes $MoO_3{\cdot}2H_2O \rightarrow MoO_3{\cdot}H_2O \rightarrow MoO_3$.

3. Angular-dispersive *versus* energy-dispersive methods

The third generation of synchrotron radiation sources, such as the European Synchrotron Radiation Facility (ESRF) in Grenoble, has opened new domains for *in-situ* studies using both angular-dispersive (monochromatic) and energy-dispersive (white radiation) powder diffraction methods. The advantage of working with constant wavelength is the much higher *d*-space resolution available which makes possible structure refinement, in particular time-resolved Rietveld analysis. The recent advent of two-dimensional position-sensitive detectors (area detectors) offers advantages over the conventional θ–2θ scans and one-dimensional position-sensitive detectors: very short exposure times with better signal to noise ratios and minimization of systematic errors.

The polymerization of disulfur dinitride, S_2N_2, into polysulfur nitride, $(SN)_x$, has been followed by combining the high flux radiation provided by the ESRF and a CCD (charge coupled device) based large area X-ray detector ($\phi = 220$ mm).[14] S_2N_2 is a highly unstable compound which polymerizes spontaneously to $(SN)_x$. This is an exceptional material exhibiting a metal-like temperature dependence of the electrical conductivity and a superconducting transition at low temperature. In order to obtain accurate crystallographic information, calibration of the detector and correction of the diffraction images are necessary. Recently developed techniques for detector calibration and processing of two-dimensional images have been used for that purpose. With exposure times of two seconds, high quality data are obtained which give the cell parameters and scale factors of the different phases in the reaction mixture, and also reliable atomic coordinates and temperature factors from Rietveld refinement of the diffraction patterns. These data show that the polymerization is preceded by a lattice distortion of S_2N_2. Determination of the atomic positions for S and N indicates retention of the reactant geometry.[15]

Resolution times on the subsecond scale have been also described, as in the case of solid combustion synthesis of TiC.[16–18] In this case the interest of the experiment was to

monitor the phase transformations of a very fast process in real time. Therefore good enough statistics to perform a Rietveld refinement were not necessary. Solid combustion synthesis usually involves high temperatures and generally releases a large amount of heat. In these types of reaction a mixture including the solid reactants is ignited by a laser or a heated tungsten coil. The combustion starts and then propagates to the whole pellet within seconds. These highly exothermic reactions maintain themselves through a combustion or reaction front. The rate of propagation can be relatively rapid (around $100\,mm\,s^{-1}$) and the temperature of the combustion front well about 2000 °C. These fast reactions have also been called self-propagating high temperature synthesis (SHS). For reviews see references 19 and 20.

Owing to the high temperatures and high rates of combustion involved in these processes, their investigation was not accomplished until recently. The investigation of the product phases has always been possible but conventional techniques do not permit determination of the dynamics and kinetics of the process taking place at the combustion front. The study of simple binary solid combustion reactions can also help. Thus, the solid combustion synthesis of TiC was monitored by using real-time angular-dispersive synchrotron radiation experiments (Fig. 2). The reaction was found to be highly exothermic and rapidly self-propagating. Because of the rapid combustion reaction synchrotron radiation was required to deal with resolution times in the subsecond range. In this particular case a diffraction pattern was taken every 200 ms. The total scan time for this experiment was 40 s. Silicon photodiode arrays were employed as position-sensitive detectors. The detector is capable of collecting a full scan of 1024 pixels in 4 ms. The specimen was ignited in a specially designed reaction cell.[17] A mixture of an equal molar ratio of Ti and amorphous carbon powders was pressed. After ignition on one edge, the reaction front propagated through the pellet. The detector was triggered at $t=0$ recording the Ti diffraction pattern at room temperature.

First of all the melting of Ti occurs (melting point 1667 °C). The disappearance of an old phase or the emergence of a new one may be easily followed by changes in the number or intensity of the diffraction peaks. At 3.6 s TiC starts to form marking the arrival of the wave front at the area of the sample

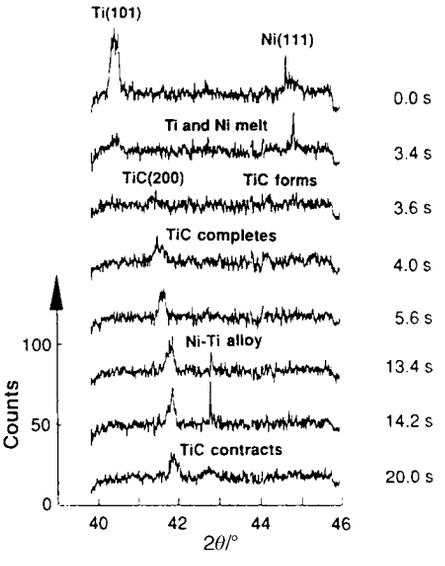

Fig. 2 Selected time-resolved synchrotron diffraction scans showing the sequence of critical events during combustion to form TiC alloy. Scan parameters: 8 keV ($\lambda=1.5497$Å), 200 ms per scan, 200 scans; $t=0$ corresponds to the triggering of the detector. Reproduced with permission from ref. 18. Copyright 1990 American Association for the Advancement of Science.

irradiated by the X-ray beam. At 4.0 s the formation of this binary phase is complete. After the reaction has reached completion the temperature gradually decreases. This fact can be observed on the shift of diffraction peaks to higher 2θ values (lattice contraction). If Ni powder is added to the initial mixture, the presence of NiTi alloy is also detected. In fact, Ni was not expected to participate in the reaction but to act as a diluent to decrease the temperature and thus to improve the time resolution of the burn. The experimental approach here described can be used to analyzed the dynamics of fast chemical reactions and to suggest models for solid combustion synthesis.

The main disadvantage of the angular dispersive method is probably the much lower flux of radiation which makes the construction of large volume reaction cells with massive sample environment apparatus difficult. In the case of the energy-dispersive X-ray diffraction technique, the entire spectral range of the radiation produced by the synchrotron source is employed. Therefore the total flux is extremely high. An energy selecting detector is used which is maintained at a fixed 2θ angle. The very high total flux and the fixed geometry of the technique facilitate the construction of bulky reaction cells with sophisticated environmental control systems. This is important since it permits the reproduction of the exact conditions required for a given chemical reaction to proceed and to be investigated *in-situ*. The main drawback of the energy-dispersive method is the low resolution of the data obtained making the structural refinement of the diffraction patterns more difficult.

Intercalation reactions and hydrothermal synthesis have benefited from the technological advances in energy-dispersive powder diffraction.[21–24] Recently O'Hare *et al.*[21,22] have reported the design of an environmental cell for measuring time-resolved energy-dispersive X-ray diffraction data for fast intercalation reactions of half-lives typically shorter than 30 min. The most significant aspect of this cell design is that it makes it possible to study a wide variety of solid–liquid processes besides intercalation reactions under normal laboratory synthetic conditions on a time scale of seconds. The experimental setup is shown in Fig. 3. In a typical kinetic experiment involving fast intercalation reactions microcrystalline samples of the metal dichalcogenide hosts are inserted into a Pyrex flask which is loaded into the diffractometer.[22] A solution of cobaltocene, $Co(\eta\text{-}C_5H_5)_2$, is then injected into the reaction vessel from a preheated reagent reservoir. Data acquisition is commenced a few seconds after stirring. The dependence of the reaction rate on the host lattice, solvent, temperature and guest concentration is studied by using this reaction cell. One of the most significant results of this experiment is the independence of the rate of intercalation on the initial cobaltocene concentration.

Combined multitechnique *in-situ* experiments are of special

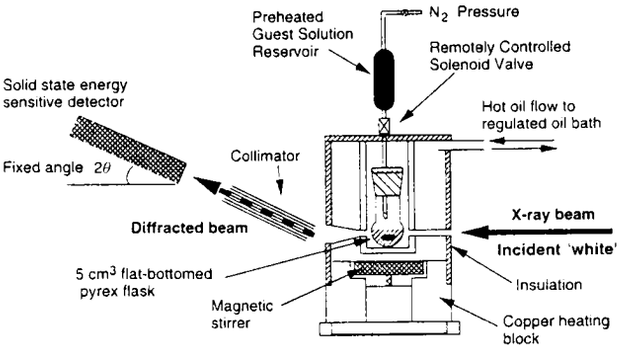

Fig. 3 Schematic diagram of the *in-situ* reaction cell used to record time-resolved energy-dispersive powder X-ray diffraction data for fast intercalation reactions. Reproduced with permission from ref. 22. Copyright 1998 American Chemical Society.

relevance since they allow a range of length scales to be probed simultaneously. Thus, *in-situ* Extended X-ray Absorption Fine Structure (EXAFS) and X-ray diffraction data collected simultaneously for the same chemical reaction provide information about both the short and long range order occurring during nucleation and crystallization.[25] This technique has been particularly powerful for *in-situ* studies of solid catalysts.[26]

4. Quantitative analysis

What is generally needed for a comprehensive description of a chemical reaction is the knowledge of the amounts of substance of all reactants present in the reaction mixture at all times. The integrated intensity of reflections for a compound in a multiphase powder diffraction pattern is related to the phase abundance in the mixture. Powder diffraction has been used for quantitative phase analysis for many years.[27] Diffraction measurements of phase abundance can be performed in many ways, but traditional methods require the acquisition of standard reference data for each phase present in the mixture to be analysed.

Although integrated line intensity and reference-intensity methods have been used for many years,[28] the Rietveld method[29,30] has been demonstrated to be very useful in devising a new and useful approach to quantitative phase analysis. Thus, Hill and Howard[31] have shown that there is a relationship between the scale factor of a given phase and its phase abundance in a mixture. The weight fraction W of a phase p is given by

$$W_p = S_p(ZMV)_p / \Sigma S_i(ZMV)_i \quad (1)$$

where S, Z, M and V are the Rietveld scale factor, the number of formula units per unit cell, the mass of the formula unit and the unit-cell volume, respectively. The summation is over all phases present. This method gives the relative weight of any component and provides an absolute weight fraction if an internal standard is introduced in a known proportion. If all phases are identified and crystalline, the sum of the weight fractions is unity and the absolute weight fractions can be obtained.

This analysis has advantages over conventional quantitative analysis methods, since no experimental precalibration is required and the use of all reflections in a pattern reduces the uncertainty in the derived weight fractions by minimizing the effects of preferred orientation and extinction. The method has been applied to mixtures containing various amounts of the cubic, tetragonal and monoclinic ZrO_2 phases[32] or to the mixture Fe_3O_4–$Li_xFe_3O_4$, of interest in solid state battery electrodes.[33] From various binary mixtures of the phases Si, SiO_2, TiO_2 and Al_2O_3 it has been shown that the crystal structure parameters and unit cell dimensions obtained for all four phases are statistically independent of their abundance in the binary mixture studied, at least down to the level of 10 wt%.[31] In particular, the atomic coordinates and thermal displacement parameters do not vary by more than 2.5 e.s.d.'s, and the unit cell dimensions are all within five e.s.d.'s. As expected, the parameter errors increase as the proportion of the phase declines in the mixture.

The method can be applied to both neutron and X-ray powder diffraction data. Neutron powder diffraction offers advantages for quantitative phase analysis over the X-ray technique in the sense that the diffraction patterns are representative of the bulk sample, rather than 'surface' regions, and absorption effects are minimized. However, when only very small quantities of sample are available the use of synchrotron radiation, for both qualitative and quantitative analysis, is particularly appropriate. This is the case of analysis of Egyptian cosmetics dating from between 2000 BC and 1200 BC.[34,35] Concerning quantitative phase analysis the samples should be free, as far as is possible, from preferred orientation.[31] The crystallites should be randomly oriented. However, for some other studies preferred orientation is found to be a useful tool of analysis (as an example, see section 7 of this article). Another approach beyond the use of the Rietveld method for quantitative analysis consists of a novel statistical tool which has been introduced to study the evolution of the structural parameters for a single phase over a wide range of temperatures. This approach has been successfully applied to the variation in the fractional occupancy of two tetrahedral orientations involved in an order–disorder phase transition.[36]

5. Kinetics

Thermodynamics as well as kinetics are important for most industrial processes. Although thermodynamics give information about the feasibility for a process to take place, it is kinetics which shows how fast a chemical reaction will proceed. In fact, for the optimization of classical processes and the development of new ones it is essential to have in-depth knowledge about the rates of the involved reactions. The study of chemical reaction kinetics by using neutron powder diffraction was initiated in the seventies.[4] This early work mainly concerns chemical or electrochemical intercalation reactions.

Usually the fraction of each crystalline phase as a function of time is calculated in order to determine the kinetic law of the transformation. In many cases the time evolution of the fraction of a phase is often represented by a phenomenological model describing the kinetics of isothermal phase transitions which proceed through nucleation and growth, also known as the JMAK model.[37] The essence of the model can be written as a very simple formula commonly referred to as the Avrami equation

$$x(t) = 1 - \exp(-kt^n) \quad (2)$$

where x is the transformed fraction, t the elapsed time, k a kinetic constant of the process which depends on temperature and n a constant related to the dimensionality of nucleation and growth. Both k and n are good experimental parameters for kinetic studies and can be determined from the intercept and slope, respectively, of a $\ln[-\ln(1-x)]$ *versus* $\ln t$ plot of the experimental data. When dealing with powder diffraction experiments, the fraction $x(t)$ can be obtained from the time evolution of the normalized intensity of a few strong reflections which are related to the considered phase (Fig. 4).[12,38,39] The value of x, the extent of reaction, as a function of time for the growth of a new crystalline phase can be calculated by using eqn. (3)

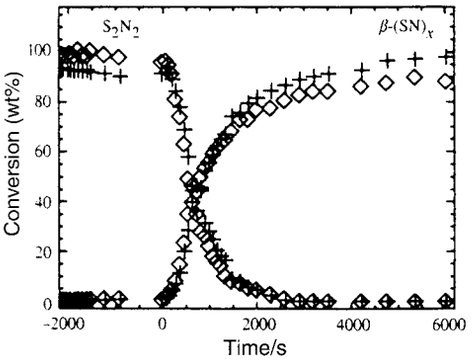

Fig. 4 Conversion *versus* time curve for S_2N_2 and formation *versus* time curve for β-$(SN)_x$. Time exposures are (+): 2 s and (◇): 20 s. Reproduced by permission of the International Union of Crystallography from ref. 14.

$$x(t) = [I_{hkl}(t)/I_{hkl}(t_\infty)] \quad (3)$$

where $I_{hkl}(t)$ is the integrated intensity of reflection *hkl* at time *t*, and $I_{hkl}(t_\infty)$ represents the integrated intensity when the chemical process is complete.

The so-called Avrami equation was derived almost simultaneously by Johnson and Mehl[40] and by Avrami;[41–43] subsequently, Erofe'ev[44] proposed that it comprises a generalized equation for the kinetics of solid-state chemical reactions. Two major types of transformation may be treated by the application of the Avrami equation. To one category belong diffusion-controlled transformations such as solid state precipitations, and to the other, diffusionless or cellular transformations typified by polymorphic transitions. The calculated value of the kinetic parameter *n* for a given process can give an idea of the type of transformation the system is experiencing. Values of *n* have been tabulated for a variety of nucleation and growth models.[45,46]

The JMAK model and particularly the Avrami equation have been applied by many workers in a range of fields including the growth of zeolite crystals[47] or polymerization in layered phosphate salts.[48] An evaluation of the phenomenological *n* parameter associated with the phase transition from the α-cobalt phthalocyanine form to the β-cobalt phthalocyanine phase indicates a 2D-growth mechanism.[38] Values of *n* in the range 1–2 in the Avrami analysis have been determined for the crystallization of $PbTiO_3$, $PbZrO_3$ and $PbZr_{0.45}Ti_{0.55}O_3$.[49] These values are consistent with preferred nucleation at surfaces and internal interfaces or diffusion-controlled growth.

Reaction kinetics of single phase and diphasic mullite gels have also been analyzed by using the Avrami equation.[50] Different reaction mechanisms are found for the two gels. Mullite formation from the single phase gel is a nucleation-controlled process with an initial formation temperature of 940 °C. However, mullite formation in the diphasic gel exhibits an Avrami type diffusion-controlled growth mechanism with the nucleation process essentially completed before substantial growth takes place. In the case of the diphasic gel, initial mullite formation temperatures are of about 1250 °C.

Recently the synthesis of microporous oxyfluorinated gallophosphate ULM-5 was performed under hydrothermal conditions from the reaction of gallium oxide, a phosphorus source, hydrofluoric acid and 1,6-diaminohexane.[23] Details of the experimental reaction cell used for these energy-dispersive experiments are given in refs. 11 and 23. When phosphoric acid is used as the phosphorus source, the kinetic analysis of time-resolved synchrotron diffraction data yields a value of $n = 0.47$, suggesting that the crystallization of ULM-5 under these conditions is a purely diffusion-controlled process independent of temperature within the range 130–200 °C. The rate of crystallization is determined only by the rate at which specimens in solution diffuse onto the nucleation point. In contrast, when phosphorus pentaoxide is employed as the phosphorus source the crystallization of ULM-5 proceeds *via* a crystalline unknown intermediate phase at a rate which is strongly dependent on temperature.

The $\ln[-\ln(1-x)]$ *versus* $\ln t$ plot for the decomposition of $BaCO_3$ in nitrogen gives the same value of the *n* parameter for temperatures within the range of 1015 to 1035 K.[51] In cases like this it is helpful to introduce the concept of an isokinetic process. During this type of process the reaction mechanism does not change within the temperature range studied. For an isokinetic process, plots of $\ln[-\ln(1-x)]$ *versus* $\ln t$ show the same slope and can be superimposed by moving the $\ln t$ axis. On the other hand if the decomposition of $BaCO_3$ as a function of time is monitored at temperatures in the range 960–1010 K, the Avrami exponent *n* changes, when compared with the value calculated for the 1015–1035 K interval of temperature, suggesting a change in the reaction mechanism. These results would indicate that the reaction mechanism associated with the decomposition of $BaCO_3$ depends on the temperature range at which the process takes place.

Following the JMAK model, a $\ln[-\ln(1-x)]$ *versus* $\ln t$ plot exhibiting a change in slope, *n*, would indicate a two-stage mechanism process. *In-situ* kinetics studies on the intercalation reaction of cobaltocene, $Co(\eta\text{-}C_5H_5)_2$, into layered dichalcogenides show that the exponent *n* changes during the course of the chemical process from $n = 2$, for the first steps of the reaction, to $n = 1$, for later stages.[22] That change in gradient in the $\ln[-\ln(1-x)]$ *versus* $\ln t$ plot can be interpreted as a transformation of the reaction mechanism as intercalation proceeds from a nucleation controlled to a diffusion controlled process.

Another relevant kinetic parameter is the activation energy E_a for a given process. An empirical estimation of E_a is given by the Arrhenius expression

$$k = k_o \exp(-E_a/k_B T) \quad (4)$$

where *k* is the reaction or process rate constant, k_o is a prefactor, k_B is the Boltzmann constant, and *T* is the absolute temperature. The prefactor k_o can be regarded as the rate constant of the process when $E_a \ll k_B T$. In contrast, if $E_a \gg k_B T$ then *k*, and the rate of the process, tend to zero. A plot of $\ln k$ *versus* $1/T$ yield values of E_a and k_o. The rate constants of a significant number of chemical process recently studied by powder diffraction methods have been found to follow Arrhenius behavior.[21,22,38,49]

Two methods of data collection are commonly used when studying the kinetics of chemical reactions: the isothermal and the non-isothermal method. The isothermal method involves heating or cooling the system under study to a temperature higher than the reaction onset temperature and then monitoring the reaction at that fixed temperature. Advantages: the methods of data analysis are well established and the parameters are well associated with a particular temperature. Disadvantages: multiple measurements are required, knowledge of the reaction onset temperature is necessary, and it is found commonly that the reaction has already commenced when the reactants are heated to the desired temperature. It is useful to note here that the Avrami equation can only be applied, strictly speaking, under constant temperature conditions. The non-isothermal method involves heating or cooling the sample at a constant rate to a temperature well beyond the reaction temperature while monitoring the reaction. This avoids the experimental problems associated with the isothermal method. For this reason methods for the analysis of non-isothermal data have been proposed.[52–54] The main drawback is that most of the non-isothermal approximations have been developed using simplifying assumptions that limit their applicability.

6. Thermal decomposition

The high incoherent background present in neutron powder diffraction patterns from samples containing hydrogen atoms is in general a serious disadvantage because it severely decreases the peak to background ratio. However, this increase of the background can be turned into an advantage in some cases like investigations dealing with dehydration/hydration of solids. The reason is that the mentioned incoherent scattering provides a direct measure of the proton content of the material under study.

A sample of cobalt(II) acetate tetrahydrate, $Co(CH_3CO_2)_2{\cdot}4H_2O$, was heated from room temperature to 600 °C and the evolution of the diffraction profile monitored by using time-resolved neutron powder diffraction.[8] At low temperature a high background intensity, due almost entirely to incoherent scattering by hydrogen, was observed (Fig. 5). By 295 °C the

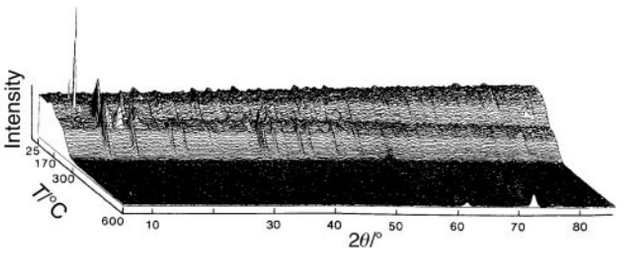

Fig. 5 Neutron diffraction profiles of $Co(CH_3CO_2)_2{\cdot}4H_2O$ decomposition as a function of heating.[8]

background is no longer present implying that there has been a complete loss of hydrogen atoms. Between 295 and 310 °C the stable phase is CoO with the zinc blende structure. The decomposition of an old phase or the emergence of a new phase may be easily followed by changes in the number or intensity of the diffraction peaks. Above 310 °C the diffraction profile is consistent with a rock-salt CoO structure. A question arises: during the process of thermal decomposition from $Co(CH_3CO_2)_2{\cdot}4H_2O$ to CoO, which is lost first, the water or the acetate group? A possible way of answering this question is repeating the experiment using cobalt(II) acetate tetrahydrate samples with selected deuterated groups. Deuterium does not create the large incoherent scattering that hydrogen does.

Thus the evolution with temperature of the neutron powder diffraction profile of a sample with deuterated acetate groups, $Co(CD_3CO_2)_2{\cdot}4H_2O$, indicates that between 100 and 155 °C there is a total loss of water molecules. In addition to the considerable difference between incoherent scattering profiles corresponding to the $Co(CH_3CO_2)_2{\cdot}4H_2O$ and $Co(CD_3CO_2)_2{\cdot}4H_2O$ samples, there is also a change in the coherently diffracted profiles. This is due to the different scattering lengths of hydrogen and deuterium, which results in different relative intensities of the diffraction peaks but does not affect the angular distribution. To investigate the temperature dependence of the acetate loss a third experiment was performed on a sample containing deuterated water molecules, $Co(CH_3CO_2)_2{\cdot}4D_2O$. The results show that the acetate loss begins at 230 °C and is complete by 295 °C. Therefore it can be concluded that during the thermal decomposition of $Co(CH_3CO_2)_2{\cdot}4H_2O$ into CoO, dehydration occurs prior to the acetate group loss.

Many naturally occurring catastrophic events, such as earthquakes and volcanic eruptions, are influenced or initiated by the behaviour of hydrous components contained within minerals. These hydrous components have a major effect upon mineral stability, behaviour and phase equilibria. The need to understand water's role in mineral behaviour makes neutron diffraction a useful technique for Earth science research. As an example, although the dehydration reaction of gypsum is a very important technical process, little is known about the reaction mechanisms and the water content of the corresponding phases. The dehydration process of gypsum as a function of temperature and time has been studied by several authors by using the incoherent scattering effect of hydrogen with the neutron beam as a measure of the water content.[55–57] Another example is provided by some copper containing minerals. The thermal behaviour of the water containing mineral volborthite $Cu_3V_2O_7(OH)_2{\cdot}2H_2O$ was studied by neutron thermodiffractometry.[58] Above 550 °C the dehydration leads to another copper containing mineral, $Cu_3V_2O_8$, called MacBirneyite. During the process of transformation, the environment of the copper atoms changes drastically from octahedral coordination, in volborthite, to square-planar and square-pyramidal coordination in MacBirneyite. Some other examples of the relevance of the high background associated with the presence of hydrogen in samples concern dehydration or water desorption processes on different types of materials.[12,59,60]

7. Texture and bones

Bone is a composite of collagen and a mineral component which is essentially hydroxyapatite, $Ca_5(PO_4)_3OH$. Since bones renew as humans and animals grow the constitution and form of a bone change during its life. In the late 19th century Wolff propounded a law: 'every change in the function of bone is followed by certain changes in its internal architecture and its external conformation'.[61,62] Bacon *et al.* tried to demonstrate the truth of this law in terms of the atomic structure of the bone by using neutron diffraction techniques.[63–66]

Neutron diffraction is a powerful technique for studying the anatomy of animal and human skeletons since neutron penetration distances are typically 1–10 mm. A bone sample corresponding to an ox femur was mounted on the D1B powder diffractometer at the Institute Laue Langevin (ILL) in Grenoble.[67] Several diffraction patterns were recorded for a variety of inclinations of the femur in relation to the neutron counter or position sensitive detector lying in the horizontal plane. A substantial preferential orientation (texture) of the *c*-axes of the hydroxyapatite along the shaft of the bone was observed when comparing the intensity of the Bragg peaks associated with the different patterns (Fig. 6). The crystal structure of this hexagonal mineral is such that for a random powder the intensities of the 002 and 111 reflections, which correspond to neighboring lines in the pattern, are roughly the same. The 111 reflection, presenting a manifold multiplicity, is nearly unaffected by preferred orientation. Therefore the 002/111 ratio of intensities deserves a measure of the degree of orientation of the *c*-axes in any chosen direction for a sample of bone.

In order to analyze the correlation between preferred orientation of the *c*-axes of $Ca_5(PO_4)_3OH$ and the age or lifestyle of the individual, Bacon *et al.*[68] performed similar neutron diffraction experiments on human femurs. They examined the enhancement of the 002 reflection as a function of age on femurs corresponding to individuals with an age ranging between one week and 82 years. The preferential orientation of the *c*-axes of the apatite crystals is low at birth and remains constant at this low value during the first year of life. Then it increases as the child grows and ceases to spend all its time lying down, reaching a maximum at an age of about 3 years when the child has become fully mobile. With further growth the orientation falls as more of life is spent sitting down. Data corresponding to the radius bone of the sheep do not show this plateau just after the birth.[69] The orientation of the *c*-axes increases continuously until it reaches a maximum value

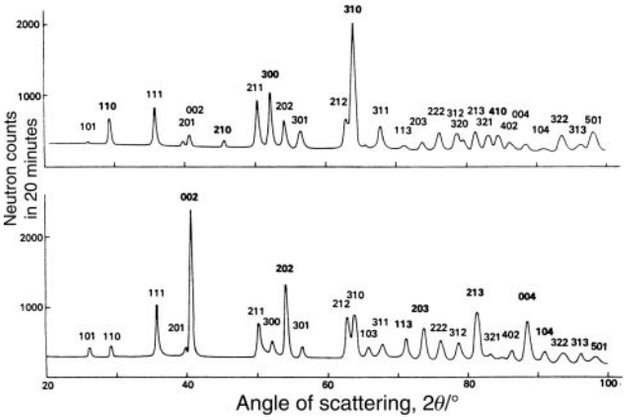

Fig. 6 Neutron diffraction patterns for the solid bone in the shaft of an ox femur recorded in 20 min at $\lambda = 2.4$ Å on the instrument D1B at ILL Grenoble. For the upper curve the bone shaft is vertical; in the lower curve the shaft is horizontal. The reflections which are notably enhanced in each pattern are indexed in heavy type. Reproduced by permission of the International Union of Crystallography from ref. 67.

for an age of about 1 year. After this age the orientation falls off but not so quickly as for a human. Sheep are animals that can stand up and run as soon as they are born. Older sheep still have to stand up a large proportion of their time.

Bacon *et al.*[70] also examined tibias belonging to human individuals from two different tribes dating from Neolithic times. One tribe lived on very hilly ground and had to work hard to carry, push and pull loads uphill. The other tribe lived on level ground. They also compared these data with data taken from present-day human tibias. From all these mentioned results Bacon *et al.* suggested that the orientation of the *c*-axes of the hydroxyapatite crystals in bones might be regarded as an imprint of the activities and lifestyle of an individual, providing an idea of the distribution of stress in the bones of the skeleton. This conclusion is in good agreement with Wolff's law. Human and animal skeletons could be regarded as mechanical constructions designed to withstand the expected forces.

A difficulty had to be solved before those experiments could be realized. The collagen in the bone contains much hydrogen which has a high incoherent neutron scattering cross section. This fact contributes to the high background of the diffraction pattern making any weak diffraction line indistinguishable. Therefore, in order to achieve any high accuracy of intensity measurement the collagen must be removed substantially. Different chemical treatments, suitable for removal of collagen without disturbance of the crystallite size and texture, were employed: i) hydrazine, ii) ethylenediamine, iii) heavy water and iv) heat for 20 min at 200, 350 and 650 °C.[65] The most satisfactory treatment was to heat the bone sample to 650 °C for 20 min. Additional measurements made with both neutrons and X-rays established that the apatite texture was not altered significantly, both crystallinity and preferential orientation, by this heat treatment which reduces the background by about nine times.

8. Estimation of particle size and microstrain during grain growth

The fact that certain chemical or physical properties depend on grain size and/or microstrain opens the fascinating possibility of tuning materials properties to desired values by adjusting those two parameters during the production process. A detail analysis of the line profile associated with the measured powder pattern can provide an estimation of the evolution of the crystallite size during the grain growth in the corresponding chemical process or give information about the presence of possible microstrains in the material. Each line profile in the powder pattern is the convolution of an instrumental line profile with a sample line profile. This additional line broadening due to sample effects results from two main effects: i) the particle-size broadening which results from the finite extent and particular morphology of the coherently diffracting domains within the grains, and ii) the microstrain broadening which results from local variations of the *d*-spacing produced by non-uniform crystalline stresses.

A size broadening analysis does not provide a measurement of the true particle size but can give a useful estimation of it. Thus, the 'apparent crystallite size' measured perpendicularly to a given (*hkl*) plane, $\langle D\rangle_{app}$, can be calculated from the well known Scherrer formula

$$\langle D\rangle_{app} = \lambda/[\beta_{sample,size}\cos\ \theta] \quad (5)$$

where λ is the wavelength used in the experiment, θ the Bragg angle associated with the (*hkl*) plane considered and β the integral breadth of the diffraction profile. The λ and θ values are straightforwardly obtained from the experimental data while $\beta_{sample,size}$ must be calculated. The subscript 'sample,size' indicates that only the contribution from size effects coming from the sample must be considered. Therefore contributions from the instrumental line profile must be removed.

The pseudo-Voigt function, pV, has been used very often to describe the peak shape of the diffraction pattern. This function is a mixture of a Lorentzian (L) and a Gaussian (G) function, $pV = \eta L + (1-\eta)G$, where $0 \leqslant \eta \leqslant 1$ is the mixing parameter.[71] In principle the instrumental contribution to the line profile can be removed by a deconvolution operation:[72]

$$\beta_{sample,L} = \beta_{exp,L} - \beta_{instr,L} \quad (6)$$

$$\beta^2_{sample,G} = \beta^2_{exp,G} - \beta^2_{instr,G} \quad (7)$$

where the subscripts 'exp', 'sample' and 'instr' refer, respectively, to the experimental, sample and instrumental profiles. Continuing with the case of a pseudo-Voigt function profile (mixing parameter η), de Keijser *et al.*[73] have obtained the following expressions:

$$\beta_L/\beta = 0.017475 + 1.500484\eta - 0.534156\eta^2 \quad (8)$$

$$\beta_G/\beta = 0.184446 + 0.812692(1-0.998497\eta)^{1/2} - 0.659603\eta + 0.44542\eta^2 \quad (9)$$

where the subscripts L and G denote, as mentioned above, the Lorentzian and Gaussian components of the pseudo-Voigt function. The integral breath β can be calculated from

$$\beta = \int I(2\theta)\, d\theta / I_{max} = w[\eta/\pi + (1-\eta)(\ln 2/\pi)^{1/2}] \quad (10)$$

where $2w$ is the full width at half maximum associated with the pV function. Eqn. (8) to 10 can be applied: i) to the experimental data collected for the material in which we are interested, in order to determine $\beta_{exp,L}$ and $\beta_{exp,G}$ and ii) to a diffraction pattern from a reference specimen in order to obtain $\beta_{instr,L}$ and $\beta_{instr,G}$. Taking into account these data together with eqn. (6) and (7), $\beta_{sample,L}$ and $\beta_{sample,G}$ can be calculated. Concerning the recording of the instrumental profile, it should be taken on a reference specimen as similar as possible to the sample compound but with no significant structural imperfections. As an example Natter *et al.*[74] have used a NIST–LaB_6 standard sample to determine the instrumental resolution of the diffractometer at the beamline BM16–Powder Diffraction of the ESRF in Grenoble (France). It is worth mentioning that, in single line analysis, the Lorentzian and Gaussian components are usually attributed to size and strain broadening respectively.[71] In that case $\beta_{sample,size} = \beta_{sample,L}$. However, in the general case, both L and G components can contribute to the particle-size broadening and therefore to $\beta_{sample,size}$ in the Scherrer formula.

The evolution of the crystallite size of MoO_3 as a function of the temperature and [*hkl*] direction has been analysed between 135 and 415 °C by using neutron powder diffraction data and the Scherrer formula.[12] MoO_3 was obtained by Boudjada *et al.*[12] as the final product of the dehydration process $MoO_3{\cdot}2H_2O \rightarrow MoO_3{\cdot}H_2O \rightarrow MoO_3$. The size broadening analysis shows that the 'apparent size' of the MoO_3 crystallites increases in preferred directions (Fig. 7). In fact the preferred direction of crystal growth is along [021]. At the beginning of the formation of MoO_3 the crystallites exhibit a marked anisotropy as a function of the crystallographic direction: the 'mean diameter' is about 150 Å in the direction perpendicular to the (001) planes, while it is only about three times smaller in the direction perpendicular to the (010) sheets. No broadening of the $MoO_3{\cdot}H_2O$ reflections was observed suggesting a much softer dehydration process $MoO_3{\cdot}2H_2O \rightarrow MoO_3{\cdot}H_2O$ when compared with $MoO_3{\cdot}H_2O \rightarrow MoO_3$.

A size broadening analysis of the line profile can be also useful to elucidate when a chemical process should be stopped in order to obtain a larger/smaller particle size. Thus, the

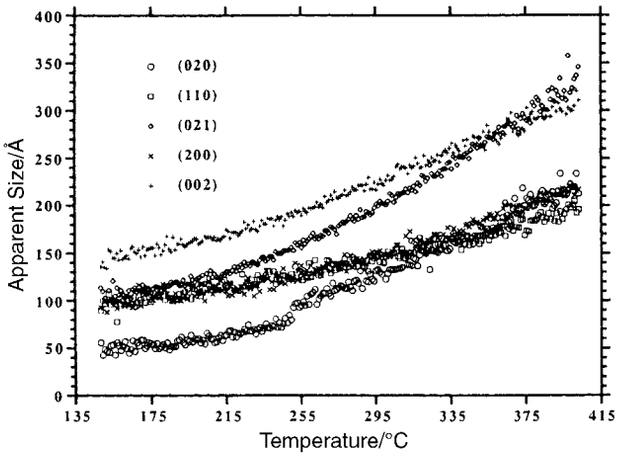

Fig. 7 Apparent crystallite size of MoO_3 in different crystallographic directions as a function of temperature. Reproduced by permission of Academic Press from ref. 12.

development of crystallization of $Fe_{80}Si_{20}$ grains with time at a fixed annealing temperature of 520 °C was followed by using the Scherrer formula.[75] The crystallization starts at times less than 2 minutes. During the first 5 minutes the 'mean grain size' increases from 6 to 10 nm. After that time the 'grain size' remains constant with a value of about 10 nm.

Another example can be found in the $PbZr_{1-x}Ti_xO_3$ (PZT) materials which are of interest for the industry due to their ferroelectric, piezoelectric, dielectric and pyroelectric properties including applications in areas such as thermal imaging, hydrophones, surface acoustic wave generators, gas sensors and nonvolatile memories. The crystallization of PZT with $x=0.0$, 0.55 and 1.0 from alkoxide gels in air has been followed by diffraction techniques at temperatures in the range 380–500 °C.[49] The 'average particle size' has been calculated by using the Scherrer equation at several temperatures showing that the crystallite size saturates to a constant value during crystallization. This saturation value increases with increasing crystallization temperature indicating a larger particle size.

Information about microstrains developed on a material during the chemical synthesis process can be also obtained from the analysis of the line profile associated with the corresponding diffraction pattern. The presence of crystalline imperfections in the sample would increase the broadening of the Bragg peaks. A Gaussian-shaped function for the 'strain profile' is an assumption subject to similar criticism as the assumption of a Lorentzian function for the 'size profile'. However, for those cases when the attribution of a Gaussian component to strain broadening is a good enough choice, then $\beta_{sample,strain}=\beta_{sample,G}$ where $\beta_{sample,G}$ can be calculated from eqn. (7), (9) and (10). The knowledge of $\beta_{sample,strain}$ makes it possible to estimate a mean local strain:[76]

$$\langle\varepsilon^2\rangle^{1/2}=2\varepsilon/(2\pi)^{1/2} \text{ where } \varepsilon=\beta_{sample,strain}\cot\theta/4 \quad (11)$$

Strain has been identified as a major contributing factor to the peak broadening revealed during the aging process of tetragonal magnesia–partially-stabilized zirconia (Mg-PSZ) at 1100 °C.[77] The process was followed by time-resolved neutron diffraction. The mechanical properties of this transformation toughening ceramic are sensitively dependent on the microstructure and phase assembly; the fabrication procedure is developed to tailor this composition and microstructure for optimum mechanical results. The strain component parallel to the *c*-axis gives a major contribution to peak broadening when compared with the degree of strain perpendicular to that direction. The reason can be found in the lenticular shape of the tetragonal Mg-PSZ. The analysis of the peak profile indicates that strain, both parallel and perpendicular to the *c*-axis, increases as the aging proceeds. A root mean square value of 0.4%/0.15% for the strain parallel/perpendicular to the *c*-axis has been determined at the end of the aging process.

Nanocrystalline iron has been prepared by pulsed electrodeposition (PED) at different temperatures and the evolution of the microstrain and grain size over more than one order of magnitude followed by *in-situ* synchrotron X-ray diffraction.[74] Owing to the extreme angular resolution of the synchrotron X-ray diffractometer the transition from the nanocrystalline regime (5–100 nm) to the polycrystalline regime (up to 500 nm) can be observed. The evolution of the microstrain with temperature and time is represented in Fig. 8. At a given temperature the microstrain decreases rapidly at the beginning of the process and then remains constant with values between 0.3% at 663 K and 0.1% at 753 K. It can be seen that the microstrain essentially disappears at 783 K.

9. Additional areas of research

In conjunction with the results discussed above, some additional areas of research are referred to in the following for the benefit of the reader: aging processes,[77] *in-situ* electrochemical reactions (batteries),[78,79] intercalation of alkanes (n-hexane, pentane, butane) in CsC_{24},[80–82] conformational changes in light- and dark-adapted membranes,[83] hydration of cements,[84,85] hydrogenation of high T_c superconductors,[86,87] orientational fluctuations in nematic liquid crystals,[88] electrolytic loading of hydrogen/deuterium into metals (palladium),[89] reactions and phase relations at mantle pressure and temperatures,[90–92] chemical synthesis by the sol–gel procedure,[93] mechanisms of phase transformation in cobalt phthalocyanine compounds,[38] 'memory effect' during polymorphic crystallizations,[94] understanding how solid catalysts work,[95] high pressure and high temperature phase transformations,[96–98] kinetics of oxidation of lanthanum strontium manganates,[99] magnesium aluminophosphate synthesis,[100] hydrothermal crystallization of zeolites,[101,102] short-lived transient states in protein molecules,[103] or natural gas conversion by CO_2 reforming.[104]

10. Concluding remarks

The usefulness of dynamic neutron and synchrotron X-ray powder diffraction methods has been stressed, presenting the current possibilities, limitations and potential of these techniques in the study of chemical processes. Such measurements provide direct information about the transformations that occur in the reactants during the progress of a reaction, thus largely contributing to understanding of the complexity of the process. Although rare, this field has been shown to be a particularly creative and promising area of research.

The choice between neutron and synchrotron radiation depends on the nature of the problem to be solved. Synchrotron radiation might be more suitable if small time resolution is required (fast

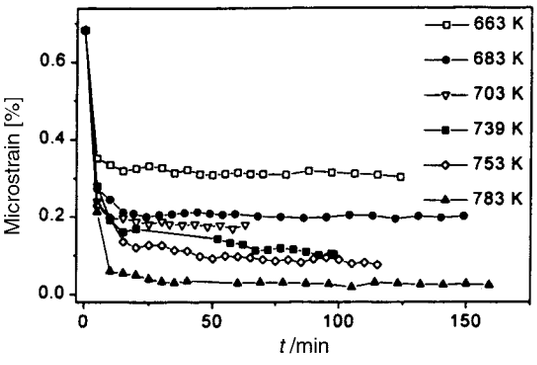

Fig. 8 Temperature and time evolution of the microstrain of nano-Fe. Reproduced with permission from ref. 74. Copyright 2000 American Chemical Society.

processes, short-live transient states), small systems available or very high pressures required (Earth's mantle pressures). However, the choice of neutrons might be more interesting for bulk analysis or for the study of chemical reactions involving mixtures of reactants which include light and heavy atoms, in particular hydration or dehydration processes.

Concerning materials chemistry, the number of areas of research to which these techniques can be applied is only limited in principle by the creativity of the researcher and the limitation of the experimental method. Therefore it can be expected that a wider range of applications will arise as more instrumental improvements (faster detectors, higher intensities and resolution, harder environment conditions, *etc.*) are available and as the imagination of scientists proposes interesting problems. In this article we have tried to discuss how materials chemistry may benefit from dynamic studies using diffraction techniques. We look forward to having encouraged further work and applications on the subject.

Acknowledgements

This work was supported by CICYT Grant No. MAT97-951. Financial support from Diputación General de Aragón (DGA) is also acknowledged.

Appendix

New generation instruments are continuously being developed. As an example D20 at the Institut Laue-Langevin (ILL) is a high-flux medium resolution powder diffractometer equipped with a large-area linear curved position-sensitive detector. D20 is used for fast data-acquisition or texture experiments. Stroboscopic measurements can be also performed. The General Materials Diffractometer (GEM) at the ISIS pulsed neutron source is a high intensity, high resolution instrument with zinc sulfide scintillator detectors covering a scattering angle from 5° to 170°. The time resolution of these modern diffractometers will be in the second and subsecond range. Current information about these instruments and others, under construction when this article was sent to the publisher, can be obtained in real time by consulting the corresponding World Wide Web sites. The electronic addresses of some Neutron and Synchrotron Facilities are listed below. Some of these (ISIS, ESRF, *etc.*) provide links to other sites supplying a more complete list.

Electronic addresses of some neutron facilities:

www.ill.fr (Institut Laue-Langevin, France)

www.isis.rl.ac.uk (ISIS pulsed neutron source, UK)

www.hmi.de/bensc (Berlin Neutron Scattering Center, BENSC, Germany)

www.pns.anl.gov (Intense Pulsed Neutron Source, IPNS, USA)

www.lansce.lanl.gov (Los Alamos Neutron Science Center, LANSCE, USA)

Electronic addresses of some synchrotron facilities:

www.esrf.fr (European Synchrotron Radiation Facility, ESRF, France)

www.srs.dl.ac.uk (CLRC synchrotron radiation source, Daresbury, UK)

www-hasylab.desy.de (HASYLAB, Germany)

www.nsls.bnl.gov (National Synchrotron Light Source, NSLS, USA)

epics.aps.anl.gov (Advanced Photon Source, APS, USA)

References

1 D. Louer, *Acta Crystallogr., Sect. A*, 1998, **54**, 922.
2 J. I. Langford and D. Louer, *Rep. Prog. Phys.*, 1996, **59**, 131.
3 A. K. Cheetham and A. P. Wilkinson, *Angew. Chem., Int. Ed. Engl.*, 1992, **31**, 1557.
4 C. Riekel, *Prog. Solid State Chem.*, 1980, **13**, 89.
5 J. Pannetier, in *Chemical Crystallography with Pulsed Neutrons and Synchrotron X-Rays*, ed. M. A. Carrondo and G. A. Jeffrey, D. Riedel Publishing Company, Dordrecht, 1988, p. 313.
6 J. Pannetier, *Chem. Scr. A*, 1986, **26**, 131.
7 J. Pannetier, *Ber. Bunsenges. Phys. Chem.*, 1986, **90**, 634.
8 R. W. Grimes and A. N. Fitch, *J. Mater. Chem.*, 1991, **1**, 461.
9 J. N. van Niekerk and F. R. L. Schoening, *Acta Crystallogr.*, 1953, **6**, 609.
10 H. Koyama and Y. Saito, *Bull. Chem. Soc. Jpn.*, 1954, **27**, 112.
11 R. I. Walton, T. Loiseau, D. O'Hare and G. Férey, *Chem. Mater.*, 1999, **11**, 3201.
12 N. Boudjada, J. Rodríguez-Carvajal, M. Anne and M. Figlarz, *J. Solid State Chem.*, 1993, **105**, 211.
13 M. Figlarz, B. Gérand, A. Delahaye-Vidal, B. Dumont, F. Harb, A. Coucou and F. Fievet, *Solid State Ionics*, 1990, **43**, 143.
14 S. O. Svensson, J. Birch, H. Müller and Å. Kvick, *J. Synchrotron Radiat.*, 1997, **4**, 83.
15 H. Müller, S. O. Svensson, J. Birch and Å. Kvick, *Inorg. Chem.*, 1997, **36**, 1488.
16 R. Frahm, J. Wong, J. B. Holt, E. M. Larson, B. Rupp and P. A. Waide, *Phys. Rev. B*, 1992, **46**, 9205.
17 E. M. Larson, P. A. Waide and J. Wong, *Rev. Sci. Instrum.*, 1991, **62**, 53.
18 J. Wong, E. M. Larson, J. B. Holt, P. A. Waide, B. Rupp and R. Frahm, *Science*, 1990, **249**, 1406.
19 A. G. Merzhanov, in *Combustion and Plasma Synthesis of High-Temperature Materials*, ed. Z. A. Munir and J. B. Holt, VCH, New York, 1990, p. 1.
20 Z. A. Munir, *Ceram. Bull.*, 1988, **27**, 342.
21 D. O'Hare, J. S. O. Evans, A. Fogg and S. O'Brien, *Polyhedron*, 2000, **19**, 297.
22 J. S. O. Evans, S. J. Price, H. V. Wong and D. O'Hare, *J. Am. Chem. Soc.*, 1998, **120**, 10837.
23 R. J. Francis, S. O'Brien, A. M. Fogg, P. S. Halasyamani, D. O'Hare, T. Loiseau and G. Férey, *J. Am. Chem. Soc.*, 1999, **121**, 1002.
24 R. J. Francis and D. O'Hare, *J. Chem. Soc., Dalton Trans.*, 1998, 3133.
25 M. Epple, G. Sankar and J. M. Thomas, *Chem. Mater.*, 1997, **9**, 3127.
26 J. M. Thomas, *Angew. Chem., Int. Ed.*, 1999, **38**, 3588.
27 G. L. Clark and D. H. Reynolds, *Ind. Eng. Chem. Anal. Ed.*, 1936, **8**, 36.
28 R. Jenkins and R. L. Snyder, *X-ray Powder Diffractometry*, John Wiley & Sons, New York, 1996.
29 R. A. Yound, *The Rietveld Method*, Oxford University Press, Oxford, UK, 1995.
30 H. M. Rietveld, *J. Appl. Crystallogr.*, 1969, **2**, 65.
31 R. J. Hill and C. J. Howard, *J. Appl. Crystallogr.*, 1987, **20**, 467.
32 C. J. Howard, E. H. Kisis, R. B. Roberts and R. J. Hill, *J. Am. Ceram. Soc.*, 1990, **73**, 2828.
33 J. Rodríguez-Carvajal and J. Fontcuberta, *J. Mater. Sci.*, 1987, **22**, 1001.
34 P. Walter, P. Martinetto, G. Tsoucaris, R. Bréniaux, M. A. Lefebvre, G. Richard, J. Talabot and E. Dooryhee, *Nature*, 1999, **397**, 483.
35 P. Martinetto, El Dooryhee, M. Anne, J. Talabot, G. Tsoucaris and Ph. Walter, *ESRF Newsletter*, 1999, **32**, 10.
36 J. S. O. Evans, W. I. F. David and A. W. Sleight, *Acta Crystallogr., Sect. B*, 1999, **55**, 333.
37 M. Fanfoni and M. Tomellini, *Il Nuovo Cimento D*, 1998, **20**, 1171.
38 P. Ballirano, R. Caminiti, C. Ercolani, A. Maras and M. A. Orru, *J. Am. Chem. Soc.*, 1998, **120**, 12798.
39 J. Rodríguez-Carvajal and J. Pannetier, in *II Curso de Difusion de Neutrones*, Centro de Estudios Avanzados del CSIC, Blanes, Spain, 1988.
40 W. A. Johnson and R. F. Mehl, *Trans. AIME*, 1939, **135**, 416.
41 M. Avrami, *J. Chem. Phys.*, 1939, **7**, 1103.
42 M. Avrami, *J. Chem. Phys.*, 1940, **8**, 212.
43 M. Avrami, *J. Chem. Phys.*, 1941, **9**, 177.
44 B. V. Erofe'ev, *C. R. (Dokl.) Acad. Sci. L'URSS*, 1946, **52**, 511.
45 S. F. Hulbert, *J. Br. Ceram. Soc.*, 1969, **6**, 11.
46 C. N. R. Rao and K. J. Rao, *Phase Transitions in Solids*, W & J Mackay Ltd., Great Britain, 1978, pp. 91–95.
47 R. W. Thompson, *Zeolites*, 1992, **12**, 680.
48 G. Cao and T. E. Mallouk, *J. Solid State Chem.*, 1991, **94**, 59.

49 A. P. Wilkinson, J. S. Speck and A. K. Cheetham, *Chem. Mater.*, 1994, **6**, 750.
50 D. X. Li and W. J. Thomson, *J. Mater. Res.*, 1990, **5**, 1963.
51 J. D. Hancock and J. H. Shrap, *J. Am. Ceram. Soc.*, 1972, **55**, 74.
52 J. A. Kennedy and S. M. Clark, *Thermochim. Acta*, 1997, **307**, 27.
53 R. R. A. Abou-Shaaban and A. P. Simonelli, *Thermochim. Acta*, 1978, **26**, 89.
54 J. Sestak, V. Stava and W. W. Wendlandt, *Thermochim. Acta*, 1973, **7**, 333.
55 P. F. Schofield, I. C. Stretton, K. S. Knight and S. Hull, *Physica B*, 1997, **234**, 942.
56 W. Abriel, K. Reisdorf and J. Pannetier, *J. Solid State Chem.*, 1990, **85**, 23.
57 A. N. Christensen, M. S. Lehmann and J. Pannetier, *J. Appl. Crystallogr.*, 1985, **18**, 170.
58 M. A. Lafontaine, G. Ferey and J. Rodríguez, *Eur. J. Solid State Inorg. Chem.*, 1990, **27**, 805.
59 P. Amorós, R. Ibañez, A. Beltrán, D. Beltrán, A. Fuertes, P. Gomez-Romero, E. Hernandez and J. Rodríguez-Carvajal, *Chem. Mater.*, 1991, **3**, 407.
60 S. Nicolopoulos, B. Lambert, M. Anne and H. Vincent, *J. Magn. Magn. Mater.*, 1990, **89**, 254.
61 J. Wolff, *Virchows Archiv fur pathologische Anatomie und Physiologie*, 1899, **155**, 256.
62 J. Wolff, *Virchows Archiv fur pathologische Anatomie und Physiologie*, 1870, **50**, 389.
63 A. C. Kitchener, G. E. Bacon and J. F. V. Vincent, *Biomimetics*, 1994, **2**, 297.
64 G. E. Bacon, P. J. Bacon and R. K. Griffiths, *J. Anat.*, 1984, **139**, 265.
65 G. E. Bacon, P. J. Bacon and R. K. Griffiths, *J. Appl. Crystallogr.*, 1979, **12**, 99.
66 G. E. Bacon, P. J. Bacon and R. K. Griffiths, *Proc. R. Soc. London, Ser. B*, 1979, **204**, 355.
67 G. E. Bacon, P. J. Bacon and R. K. Griffiths, *J. Appl. Crystallogr.*, 1977, **10**, 124.
68 G. E. Bacon and R. K. Griffiths, *J. Anat.*, 1985, **143**, 97.
69 G. E. Bacon and A. E. Goodship, *J. Anat.*, 1991, **179**, 15.
70 G. E. Bacon, *Proc. R. Soc. London, Ser. B*, 1990, **240**, 363.
71 Th. H. de Keijser, J. I. Langford, E. J. Mittemeijer and A. B. P. Vogels, *J. Appl. Crystallogr.*, 1983, **16**, 309.
72 J. Il Langford, *J. Appl. Crystallogr.*, 1978, **11**, 10.
73 Th. H. de Keijser, E. J. Mittemeijer and H. C. F. Rozendaal, *J. Appl. Crystallogr.*, 1983, **15**, 308.
74 H. Natter, M. Schmelzer, M. S. Löffler, E. E. Krill, A. Fitch and R. Hempelmann, *J. Phys. Chem. B*, 2000, **104**, 2467.
75 G. Hampel, A. Pundt and J. Hesse, *J. Phys.: Condens. Matter.*, 1992, **4**, 3195.
76 R. Delhez, Th. H. Keijser and E. J. Mittemeijer, *Fresenius Z. Anal. Chem.*, 1982, **312**, 459.
77 D. N. Argyriou, C. J. Howard and R. I. Smith, *J. Am. Ceram. Soc.*, 1994, **77**, 12.
78 Y. Chabre and J. Pannetier, *Progr. Solid State Chem.*, 1995, **23**, 1.
79 M. Latroche, A. Percheron-Guégan, Y. Chabre, J. Bouet, J. Pannetier and E. Ressouche, *J. Alloys Compd.*, 1995, **231**, 537.
80 F. Beguin and H. Pilliere, *Carbon*, 1998, **36**, 1759.
81 A. M. Balagurov, E. P. Kozlova, G. M. Mironova and I. Jacyna-Onyszkiewicz, *Phys. Status Solidi A*, 1993, **136**, 57.
82 M. Goldmann, J. Pannetier, F. Beguin and B. Gonzalez, *Synth. Met.*, 1988, **23**, 133.
83 N. A. Dencher, G. Papadopoulos, D. Dreselhauss and G. Buldt, *Biochim. Biophys. Acta*, 1990, **1026**, 51.
84 A. C. Jupe, S. Turrillas, P. Barnes, S. L. Colston, C. Hall, D. Haüsermann and M. Hanfland, *Phys. Rev. B*, 1996, **53**, R14697.
85 P. Barnes, *J. Phys. Chem. Solids*, 1991, **52**, 1299.
86 A. M. Balagurov, G. M. Mironova, L. A. Rudnickij and V. Ju.Galkin, *Physica C*, 1990, **172**, 331.
87 D. Fruchart, J. L. Soubeyroux, D. Tran Qui, C. Pique, C. Rillo, F. Lera, V. Orera, J. Flokstra and H. A. Blank, *J. Less Common Met.*, 1990, **157**, 233.
88 T. Riste and K. Otnes, *Liq. Cryst.*, 1993, **14**, 581.
89 R. Mukhopadhyay, B. A. Dasannacharya, D. Nandan, A. J. Singh and R. M. Iyer, *Solid State Commun.*, 1990, **75**, 359.
90 N. J. Chinnery, A. R. Pawley and S. M. Clark, *Science*, 1999, **286**, 940.
91 C. Meade, H. K. Mao and J. Hu, *Science*, 1995, **268**, 1743.
92 S. K. Saxena, L. S. Dubrovinsky, P. Haggkvist, Y. Cerenius, G. Shen and H. K. Mao, *Science*, 1995, **269**, 1703.
93 A. K. Cheetham and C. F. Mellot, *Chem. Mater.*, 1997, **9**, 2269.
94 L. F. Barquin, J. M. Barandiaran, I. Telleria and J. C. Gómez Sal, *Phys. Status Solidi A*, 1996, **155**, 439.
95 L. Smith, A. K. Cheetham, R. E. Morris, L. Marchese, J. M. Thomas, P. A. Wright and J. Chen, *Science*, 1996, **271**, 799.
96 S. Hull, C. A. Keen, W. Hayes and N. J. G. Gardner, *J. Phys.: Condens. Matter*, 1998, **10**, 10941.
97 S. Hull and D. A. Keen, *Phys. Rev. B*, 1999, **59**, 750.
98 S. Hull and P. Berastegui, *J. Phys.: Condens. Matter*, 1999, **11**, 5257.
99 E. K. Andersen, I. G. K. Andersen, P. Norby and J. C. Hanson, *J. Solid State Chem.*, 1998, **141**, 235.
100 A. N. Christensen, P. Norby and J. C. Hanson, *Acta Chem. Scand.*, 1997, **51**, 249.
101 P. Norby, *J. Am. Chem. Soc.*, 1997, **119**, 5215.
102 S. Ueno, A. Minato, H. Seto, Y. Amemiya and K. Sato, *J. Phys. Chem. B*, 1997, **101**, 6847.
103 H. D. Bartunik, *Rev. Phys. Appl.*, 1984, **19**, 671.
104 A. T. Ashcroft, A. K. Cheetham, R. H. Jones, S. Natarajan, J. M. Thomas, D. Waller and S. M. Clark, *J. Phys. Chem.*, 1993, **97**, 3355.